scientific reports

Check for updates

OPEN

Unprecedently large $^{37}Cl/^{35}Cl$ equilibrium isotopic fractionation on nano-confinement of chloride anion

Mateusz Pokora[1], Agata Paneth[2] & Piotr Paneth[1,3]✉

Confinement can result in unusual properties leading to new, exciting discoveries in the nano-realm. One such consequence of confinement at the nanoscale is extremally large isotopic fractionation, especially at sub-van der Waals distances. Herein, on the example of chlorine isotope effects, we show that at conditions of nanoencapsulation these effects may reach values by far larger than observed for the bulk environment, which in the case of nanotubes can lead to practical applications (e.g., in isotopic enrichment) and needs to be considered in analytical procedures that employ nanomaterials.

Many physicochemical properties change dramatically at the nanoscale compared to bulk properties. A number of these differences originate in the confinement of the molecules in nano or sub-nano structures. Sulfur allotropy[1], change in electrochemical reactivity[2], and ferroelectric properties of polymers in narrow nanotubes[3], solar cell operations[4], liquid crystals properties in microdroplets[5], hydrogen atom transfer in micelles[6], or glass transitions in mesoporous nanochannels[7], are among recently described examples of such phenomena. Confinement, by influencing molecular vibrations[8–10], can also lead to isotopic fractionation. While the change of properties of water confined in nanotubes has been documented some time ago[11] it is only recently that the related deuterium isotope effects have been reported[12,13]. Kinetics and equilibrium deuterium isotope effects on the confinement at the macroscale have also been observed in the past[14–17]. They are, however, much larger than heavy-atom[18] isotope effects which have neither been measured nor predicted thus far (although they were recently reported for conductivity[19] and diffusion[20]).

Chlorine isotopic fractionation is a very informative tool used in many life-controlling processes[21], including environmental[22–25], geochemical[26–30] and biochemical[31–33] studies. Therefore a detailed understanding of this phenomenon is an important scientific (but with practical consequences in the interpretation of experimental results[34] and analytical techniques[35–37]) issue. It is thus not surprising that studies on model reactions[38] and theoretical predictions have been performed[33,34,39–41]. In our recent studies[42], we have shown that noncovalent chlorine isotope effects can be correlated with the hydrogen bond strength. However, even when hydrogen bonds were approaching a very weak region the isotope effects, albeit small, did not disappear. We have, therefore, attempted to investigate the sources of this "residual" chlorine isotopic fractionation with the assumption that it originates in van der Waals interactions, and following our studies of the adsorption on the graphene[43], we have initially considered chloride anion adsorbed on graphene. The isotope effect was not alleviated completely, which prompted us to study isotopic consequences of chloride interactions with other nanostructures. We have observed that encapsulation leads to values by far larger than any value observed at the bulk scale where the largest chlorine kinetic isotope effects are expected not to exceed about 25 ‰ (expressed as the deviation from unity, see Eq. (2))[41]. In this contribution, we present the results of chlorine isotope effects of chloride trapped in different nanostructures and show their surprisingly large values and their relation to the distance to the surrounding environment. For comparison, micro-solvated chloride in nanotubes, as well as boron-nitrogen[44] and gold[45] cages have been considered.

[1]International Center for Research on Innovative Biobased Materials (ICRI-BioM) – International Research Agenda, Lodz University of Technology, Żeromskiego 116, 90-924 Lodz, Poland. [2]Department of Organic Chemistry, Faculty of Pharmacy, Medical University of Lublin, Chodźki 4a, 20-093 Lublin, Poland. [3]Institute of Applied Radiation Chemistry, Faculty of Chemistry, Lodz University of Technology, Żeromskiego 116, 90-924 Lodz, Poland. ✉email: piotr.paneth@p.lodz.pl

Structure	Minimal Distance, Å	^{37}Cl-EIE	ε^{37}Cl, ‰
F20	1.65	0.95700	44.9
F30	2.03	0.97412	26.6
F60	3.52	0.99769	2.3
N10-8	1.85	0.97469	25.0
N12-7	1.73	0.97148	29.4
N12-10	1.73	0.97174	29.1
N12-14	1.75	0.97189	28.9
N12-14 + 1aq	1.79	0.97447	26.2
N12-14 + 2aq	1.80	0.97220	28.6
N16-9	2.77	0.98952	10.6
N20-10	3.78	0.99953	0.5
B19N19	2.50	0.98610	14.1
Au20	2.73	0.99527	4.8
G54	3.21	0.99941	0.6

Table 1. Minimal X-Cl (X = C, N, B, or Au) distances, equilibrium isotope effects and isotopic fractionations.

Theoretical methods

Geometries of all considered structures have been first optimized in the gas phase to the nearest energy minimum at the DFT level of theory, using ωB97X-D functional[46] (which includes G2 Grimme dispersion correction for all atoms treated explicitly) expressed in the def2-TZVP basis set[47] as implemented in the Gaussian16 program[48]. Default convergence criteria have been applied. They are available in the Supplementary Information. Vibrational analysis has been used to ensure that the optimized geometry corresponds to a stationary point representing a minimum on the potential energy surface (3n-6 real vibrations). The influence of the inclusion of the counterpoise correction[49] for the basis set superposition error (BSSE) has been found to be negligible (Table 2). SMD Polarized Continuum Model of solvent with parameters for the aqueous solution (which includes dispersion correction in the CDS part that applies to the bulk properties of the solvent) has been used[50]. Chlorine equilibrium isotope effects, ^{37}Cl-EIE, were calculated at 298 K according to the Bigeleisen equation which relates an isotope effect to vibrational frequencies[51]:

$$\mathrm{EIE} = \prod_{i}^{3n_R-6} \frac{u_{Ri}^{H} \cdot \sinh\left(\frac{u_{Ri}^{L}}{2}\right)}{u_{Ri}^{L} \cdot \sinh\left(\frac{u_{Ri}^{H}}{2}\right)} \Bigg/ \prod_{i}^{3n_P-6} \frac{u_{Pi}^{H} \cdot \sinh\left(\frac{u_{Pi}^{L}}{2}\right)}{u_{Pi}^{L} \cdot \sinh\left(\frac{u_{Pi}^{H}}{2}\right)} \tag{1}$$

in which R and P denote reactant and product, respectively, n is the number of atoms, $u_i = h\nu_i/k_BT$, where h and k_B are Planck and Boltzmann constants, respectively, T is absolute temperature, and ν_i are the frequencies of normal modes of vibrations. Calculations were performed using harmonic frequencies with the aid of the Isoeff program[52].

Results and discussion

To find out the influence of confinement five nanotubes of different lengths and radius, and three different fullerenes were studied. The graphene sheet was used as the reference that does not impose any confinement. The studied structures are collected in Table 1 which also introduces symbols used; the letter indicates the type; G—graphene, N—nanotubes, and F—fullerene. For G and F types the number corresponds to the number of carbon atoms. In the case of nanotubes, the first digits represent the number of carbon atoms in the cross-section and thus provide information on the structure diameter while the second defines the length of the model (compare **N12-7**, **N12-10**, and **N12-14** in Fig. 1). Additionally, we have tested the influence of the type of elements that form the cage. For this purpose, we used a tetrahedral gold pyramid of 20 atoms and a fullerene-type cage formed by 19 nitrogen and 19 boron atoms.

Since chlorine equilibrium isotope effects, ^{37}Cl-EIE, are very small, the results are presented as isotopic fractionation factors, ε, which express an isotope effect as the deviation from unity in "per-mil" units [‰] (that correspond to mUr of the SI system):

$$\varepsilon^{37}\mathrm{Cl} = \left[1/^{37}\mathrm{Cl\text{-}EIE} - 1\right] * 1000 \tag{2}$$

In this notation, negative values correspond to isotope effects larger than unity (so-called normal isotope effects) while positive values correspond to isotope effects smaller than unity (so-called inverse isotope effects).

We have employed hybrid density functional from the family that has been shown successful in modeling non-covalent interactions in the recent benchmark studies[53]. The obtained results for the equilibrium between chloride anion in the gas phase and nano-environment are illustrated in Fig. 3, which represents the dependence of ε^{37}Cl on the distance between chloride anion and nearest atom of the nano-structure. The corresponding numerical results are collected in Table 1. As can be seen, it increases exponentially (the dotted blue line illustrates this trend) when the distance becomes smaller. The green line in this figure corresponds to ^{37}Cl-EIE on

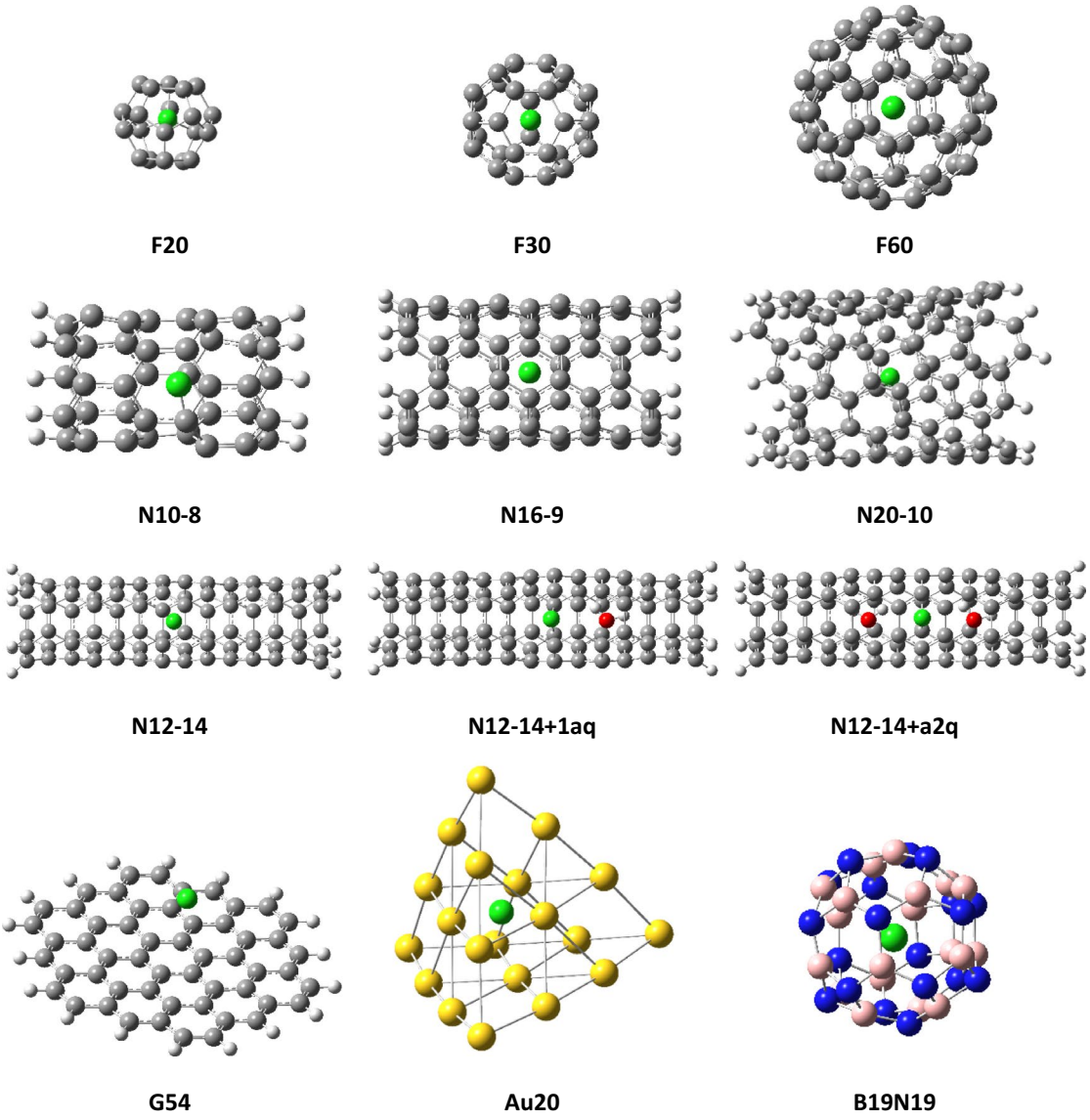

Figure 1. Nanostructures used in modeling of chlorine isotope effects.

the putative equilibrium between chloride ion and its incorporation into a C–Cl covalent bond in the gas phase, which marks the maximum equilibrium isotope effect in the bulk of about 9 ‰ (the green line in Fig. 2). Within this limit, only ε^{37}Cl of complexes without serious spatial constraints are contained (e.g., **F60**). For chloride confined in small fullerenes (e.g., **F30**) or narrow nanotubes (e.g., **N10**), the distances to the closest nanostructure are small and the resulting isotopic fractionation reaches values significantly larger than those encountered in a bulk environment. In fact, in the absolute sense, they are larger than the values of the largest expected chlorine kinetic isotope effects (about 24.3 ‰[41]). Even larger isotopic fractionation is observed when confinement results in covalent interactions (e.g., **F20**).

Isotope effects and thus corresponding isotopic fractionations arise from differences in isotopic vibrations. We have analyzed contributions from individual frequencies to the overall calculated EIE on the examples representing different nanostructures (graphene, **G54**, nanotube, **N16-9**, and fullerene, **F30**) and the whole range of the isotopic fractionation (compare entries in Table 1). In all cases, only a few frequencies exhibit a shift upon substitution of ^{35}Cl by ^{37}Cl, with three vibrations along three coordinate axes involving chloride displacement exhibiting the largest isotopic shift as illustrated by Fig. 3 on the example of **F30**. These frequencies, together with corresponding force constants are collected in Table 2 (complete lists of isotopic frequencies for these structures are provided in the Supplementary Information, Tables S15–S17).

Additionally, frequencies and force constants associated with vibrations involving the carbon atom closest to the chloride and its distances to the neighboring carbon atoms are listed. A comparison of the properties with the structure without the chloride is also provided in Table 2. As can be seen from the comparison of the last two rows the C–C distances of the carbon atom that is closest to the chloride anion are shorter indicating that encapsulation leads to a swelling of the nanostructure. The vibrational pattern in which this atom participates also changes, however, these modes are not isotope sensitive so they do not affect the isotopic fractionation.

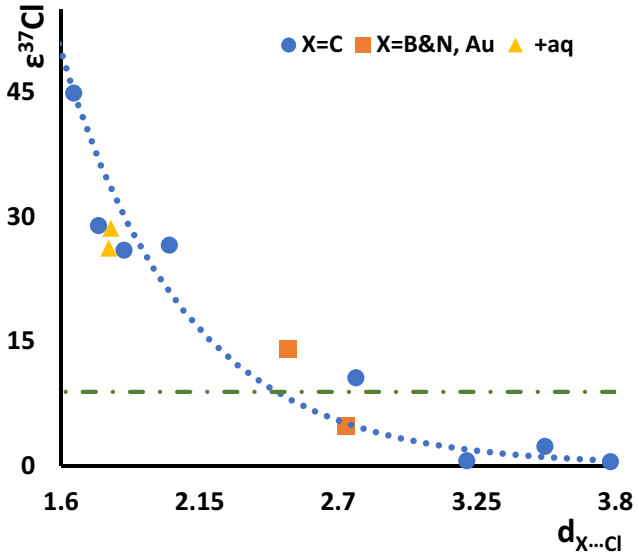

Figure 2. Dependence of the chlorine isotopic fractionation (ε^{37}Cl in ‰) on the distance ($d_{X\cdots Cl}$ in Å) of chloride from the nearest atom of the nanostructure. Blue circles refer to the distance from the carbon atom. Yellow triangles refer to the distance from the carbon atom in cases with continuum models of solvent included. Distances from Au and B are represented by orange squares (see Table 1 for numerical values). The green line at about 9 ‰ corresponds to the maximum equilibrium isotope effect.

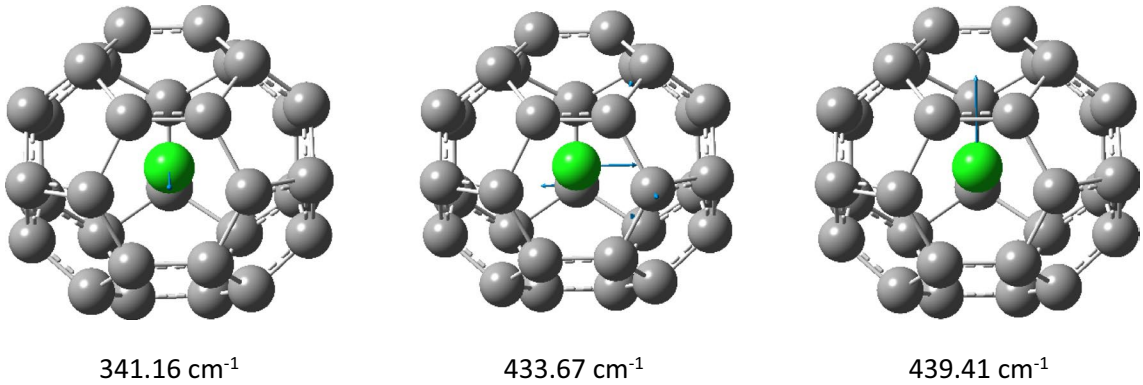

Figure 3. Displacement vectors of the three most isotope-sensitive vibrations.

Structure	Atom	Frequencies/Force constants			Cl–C and C–C distances		
G54	Cl	$11.30/0.00_2$	$21.71/0.00_7$	104.03/0.07	3.21		
	C(9)	$395.70/0.51$	$759.94/2.09$	$1453.8/12.21$	1.42_3	1.40_3	1.40_5
G54 no Cl⁻		$773.31/3.07$	$774.80/2.12$	$1449.49/12.71$	1.42_5	1.40_6	1.40_7
N16-9	Cl	63.90/0.07	296.22/0.90	296.54/0.90	2.77		
	C(23)	$594.13/1.13$	$684.75/2.98$	$1291.16/9.92$	1.43_8	1.43_5	1.41
N16-9 no Cl⁻		$727.46/1.97$	$1509.17/13.82$	$1614.77/17.90$	1.43_6	1.43_6	1.39
F30	Cl	341.16/1.59	433.67/1.84	439.41/2.54	2.03		
	C(16)	$90.92/0.06$	$560.44/2.25$	$1249.16/11.04$	1.53	1.48	1.48
F30 no Cl⁻		$728.02/3.75$	$1280.09/11.59$	$1348.99/12.87$	1.45	1.44	1.44

Table 2. Vibrational analysis of normal modes associated with chlorine atom and its nearest carbon neighbor. Frequencies in cm^{-1}, force constants in mdyne/Å, distances in Å. Numbering of carbon atoms corresponds to structures provided in the respective table of the Supplementary Information.

Property	Minimal distance, Å	^{37}Cl-EIE	ε^{37}Cl [‰]
Gas phase	2.77176	0.98952	10.59
Counterpoise	2.77178	0.98958	10.53
Implicit PCM SMD	2.77181	0.99057	9.52

Table 3. Influence of counterpoise BSSE correction and continuum solvent model.

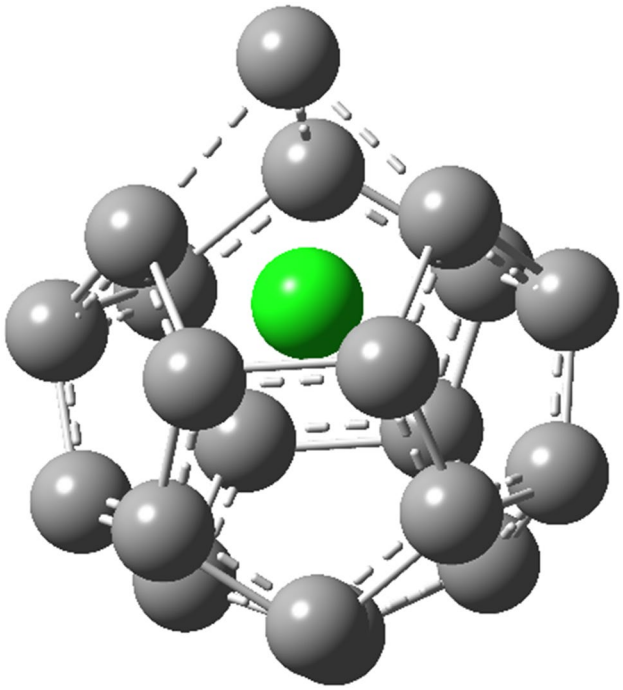

Figure 4. Structure of chloride encapsulated in **F20**.

Thus far we have considered isotopic fractionation on the equilibrium between chloride anion isolated in the gas phase and the nano-environment. Equally, or maybe even more important, is the transfer from the condensed phase, in particular from the aqueous solution since the nano-environment has a significant influence on the properties of water and solvation[54,55]. In such cases, the values reported in Table 2 and Fig. 3 are smaller by about 4 ‰ which corresponds to the chlorine isotopic fractionation on the transfer of chloride anion from the gas phase to the aqueous solution[42]. On the example of **N16-9** we show, however, that the use of the continuum solvent model underestimates the effect of the polar environment, leading to the ε^{37}Cl value lower by only about 1 ‰ – compare entries in the first and third raw of Table 3.

To study the effect of micro-solvation in nanotubes one or two water molecules have been added to the **N12-14** model. For these studies, it was necessary to use the elongated nanostructures to confine water molecules within the hydrophobic environment of the nanotube. As expected, and evidenced by values collected in Table 3, the elongation of the nanotube has a negligible influence on the isotopic fractionation (compare results for **N12-7**, **N12-10**, and **N12-14** in Table 3). The obtained values indicate that micro-solvation has also a negligible effect on chlorine isotopic fractionation and does not alleviate its enormous enhancement caused by the confinement.

The extreme case of **F20** deserves additional analysis. In this case, chloride does not occupy the center of the nanostructure but is shifted 0.6 Å toward the edge, which causes elongation of bonds to the carbon atom which is pushed out by about 0.45 Å as illustrated by Fig. 4. The chloride anion position is stiffened by interactions with three neighboring carbon atoms, which are at practically covalent distances (1.65 Å). Thus the source of this huge isotopic fractionation goes beyond a simple effect of encapsulation.

Finally, energy aspects need to be considered. Structures in which chloride is caged within a nanostructure, i.e., systems other than nanotubes, are of no practical relevance regarding their exploitation for isotopic enrichment since the encapsulation energy is high and the formation of these structures requires the opening of a "window" in the nanostructure[56,57], which usually requires harsh conditions and about 80 kcal/mol[58] although lower energies might suffice in the case of functionalized structures.

Conclusions

The most important conclusion of the present studies is, exemplified by the calculations on chloride anion in nano-environment, extremely large isotopic fractionation caused by the confinement in constrained structures. Furthermore, solvation with even such polar solvents as water has only a minor effect on this phenomenon. This observation can lead to new methods of isotopic enrichment, especially for systems/elements which exhibit small isotopic fractionation under bulk conditions. More importantly, it also calls for special caution in the interpretation of experimental protocols of purification of material for isotopic ratio measurements as well as procedures used in these analyses.

Data availability

The optimized structures used in this study are available in Supplementary Tables S1 to S14. Tables S15 to S17 provide isotopic frequencies for structures **F30**, **N16-9**, and **G54**, respectively.

Received: 17 August 2021; Accepted: 14 January 2022
Published online: 02 February 2022

References

1. Xin, S. *et al.* Smaller sulfur molecules promise better lithium-sulfur batteries. *J. Am. Chem. Soc.* **134**, 18510–18513 (2012).
2. Fu, C. *et al.* Confined lithium-sulfur reactions in narrow-diameter carbon nanotubes reveal enhanced electrochemical reactivity. *ACS Nano* **12**, 9775–9784 (2018).
3. Martín, J. *et al.* Relaxations and relaxor-ferroelectric-like response of nanotubularly confined poly(vinylidene fluoride). *Chem. Mater.* **29**, 3515–3525 (2017).
4. Kamat, P. V. & Kuno, M. Halide ion migration in perovskite nanocrystals and nanostructures. *Acc. Chem. Res.* **54**, 520–531 (2021).
5. Chen, H.-Q., Wang, X.-Y., Bisoyi, H. K., Chen, L.-J. & Li, Q. Liquid crystals in curved confined geometries: Microfluidics bring new capabilities for photonic applications and beyond. *Langmuir* **37**, 3789–3807 (2021).
6. Miller, S. L., Wiebenga-Sanford, B. P., Rithner, C. D. & Levinger, N. E. Nanoconfinement raises the energy barrier to hydrogen atom exchange between water and glucose. *J. Phys. Chem. B* **125**, 3364–3373 (2021).
7. Abdel Hamid, A. R. *et al.* Multiple glass transitions of microphase separed binary liquids confined in MCM-41. *J. Phys. Chem. C* **120**, 11049–11053 (2016).
8. Sadhukhan, M. & Tkatchenko, A. Long-range repulsion between spatially confined van der Waals dimers. *Phys. Rev. Lett.* **118**, 210402 (2017).
9. Zaleśny, R., Chołuj, M., Kozłowska, J., Bartkowiak, W. & Luis, J. M. Vibrational nonlinear optical properties of spatially confined weakly bound complexes. *Phys. Chem. Chem. Phys.* **19**, 24276–24283 (2017).
10. Podeszwa, R. & Jansen, G. Comment on 'long-range repulsion between spatially confined van der Waals dimers'. *Phys. Rev. Lett.* **120**, 258901 (2018).
11. Tadokoro, M. *et al.* Anomalous water molecules and mechanistic effects of water nanotube clusters confined to molecular porous crystals. *J. Phys. Chem. B* **114**, 2091–2099 (2010).
12. Mawatari, K., Isogai, K., Morikawa, K., Ushiyama, H. & Kitamori, T. Isotope effect in the liquid properties of water confined in 100 nm nanofluidic channels. *J. Phys. Chem. B* **125**, 3178–3183 (2021).
13. Zhan, Y.-Y. *et al.* Polarizability and isotope effects on dispersion interactions in water. *Commun. Chem.* **2**, 1–8 (2019).
14. Zhao, Y.-L., Houk, K. N., Rechavi, D., Scarso, A. & Rebek, J. Equilibrium isotope effects as a probe of nonbonding attractions. *J. Am. Chem. Soc.* **126**, 11428–11429 (2004).
15. Rechavi, D., Scarso, A. & Rebek, J. isotopomer encapsulation in a cylindrical molecular capsule: A probe for understanding non-covalent isotope effects on a molecular level. *J. Am. Chem. Soc.* **126**, 7738–7739 (2004).
16. Haino, T., Fukuta, K., Iwamoto, H. & Iwata, S. Noncovalent isotope effect for guest encapsulation in self-assembled molecular capsules. *Chemistry* **15**, 13286–13290 (2009).
17. Muhammad, R. *et al.* Exploiting the specific isotope-selective adsorption of metal-organic framework for hydrogen isotope separation. *J. Am. Chem. Soc.* https://doi.org/10.1021/jacs.1c01694 (2021).
18. Paneth, P. Theoretical calculations of heavy-atom isotope effects. *Comput. Chem.* **19**, 231–240 (1995).
19. Nguyen, Q. V. & Frisbie, C. D. Hopping conductance in molecular wires exhibits a large heavy-atom kinetic isotope effect. *J. Am. Chem. Soc.* **143**, 2638–2643 (2021).
20. Fortin, M.-A., Watson, E. B. & Stern, R. The isotope mass effect on chlorine diffusion in dacite melt, with implications for fractionation during bubble growth. *Earth Planet. Sci. Lett.* **480**, 15–24 (2017).
21. Russell, J. M. & Boron, W. F. Role of chloride transport in regulation of intracellular pH. *Nature* **264**, 73–74 (1976).
22. Reddy, C. M. *et al.* Stable chlorine intramolecular kinetic isotope effects from the abiotic dehydrochlorination of DDT. *Environ. Sci. Pollut. Res. Int.* **9**, 183–186 (2002).
23. Lihl, C. *et al.* Compound-specific chlorine isotope fractionation in biodegradation of atrazine. *Environ. Sci.* **22**, 792–801 (2020).
24. Liu, Y., Parks, F. C., Sheetz, E. G., Chen, C.-H. & Flood, A. H. Polarity-tolerant chloride binding in foldamer capsules by programmed solvent-exclusion. *J. Am. Chem. Soc.* **143**, 3191–3204 (2021).
25. Drenzek, N. J. *et al.* Invariant chlorine isotopic signatures during microbial PCB reductive dechlorination. *Environ. Pollut.* **128**, 445–448 (2004).
26. Gascoyne, M. *Chlorine isotopes and their application to groundwater dating at Olkiluoto* 21 (2014).
27. Sherif, M. I., Sultan, M. & Sturchio, N. C. Chlorine isotopes as tracers of solute origin and age of groundwaters from the Eastern Desert of Egypt. *Earth Planet. Sci. Lett.* **510**, 37–44 (2019).
28. Agrinier, P. *et al. Chlorine Stable Isotope Ratios (35Cl/37Cl) of Chlorides of Fluids Produced in Low Permeability Clay-Rich Sediments: The Potential Role Ion Filtration* (European Association of Geoscientists & Engineers, 2018).
29. Agrinier, P. *et al.* Strong impact of ion filtration on the isotopic composition of chlorine in young clay-rich oceanic sediment pore fluids. *Geochim. Cosmochim. Acta* **245**, 525–541 (2019).
30. Agrinier, P. *et al.* Chlorine isotope data of chlorides challenge the pore fluid paradigm. *Geochim. Cosmochim. Acta* **300**, 258–278 (2021).
31. Paneth, P. Chlorine kinetic isotope effects on enzymatic dehalogenations. *Acc. Chem. Res.* **36**, 120–126 (2003).
32. Paneth, P. Chlorine isotope effects in biological systems. In *Isotope Effects in Chemistry and Biology* (eds Kohen, A. & Limbach, H.-H.) 875–891 (Taylor & Francis, 2006).
33. Sicinska, D., Rostkowski, M. & Paneth, P. Chlorine isotope effects on chemical reactions. *Curr. Org. Chem.* **9**, 75–88 (2005).
34. Siwek, A. *et al.* Binding modes of DL-2-haloacid dehalogenase revealed by crystallography, modeling and isotope effects studies. *Arch. Biochem. Biophys.* **540**, 26–32 (2013).

35. Szatkowski, L. *et al.* Chapter Eight: Measurement and prediction of chlorine kinetic isotope effects in enzymatic systems. In *Methods in Enzymology* Vol. 596 (eds Harris, M. E. & Anderson, V. E.) 179–215 (Academic Press, 2017).
36. Westaway, K. C., Koerner, T., Fang, Y. R., Rudziński, J. & Paneth, P. A new method of determining chlorine kinetic isotope effects. *Anal. Chem.* **70**, 3548–3552 (1998).
37. Julien, M., Liégeois, M., Höhener, P., Paneth, P. & Remaud, G. S. Intramolecular non-covalent isotope effects at natural abundance associated with the migration of paracetamol in solid matrices during liquid chromatography. *J. Chromatogr. A* **1639**, 461932 (2021).
38. Giunta, T., Labidi, J. & Eggenkamp, H. G. M. Chlorine isotope fractionation between chloride (Cl−) and dichlorine (Cl2). *Geochim. Cosmochim. Acta* **213**, 375–382 (2017).
39. Schauble, E. A., Rossman, G. R. & Taylor, H. P. Theoretical estimates of equilibrium chlorine-isotope fractionations. *Geochim. Cosmochim. Acta* **17**, 3267–3281 (2003).
40. Czarnacki, M. & Hałas, S. Isotope fractionation in aqua-gas systems: Cl2-HCl-Cl−, Br 2-HBr-Br− and H2S–S2−. *Isot. Environ. Health Stud.* **48**, 55–64 (2012).
41. Świderek, K. & Paneth, P. Extending limits of chlorine kinetic isotope effects. *J. Org. Chem.* **77**, 5120–5124 (2012).
42. Paneth, A. & Paneth, P. Isotopic consequences of host-guest interactions; noncovalent chlorine isotope effects. *J. Phys. Chem. B* **125**, 1874–1880 (2021).
43. Pokora, M. & Paneth, P. Can adsorption on graphene be used for isotopic enrichment? A DFT perspective. *Molecules* **23**, 2981 (2018).
44. Li, R. & Wang, Y. Modification of boron nitride nanocages by titanium doping results unexpectedly in exohedral complexes. *Nat. Commun.* **10**, 4908 (2019).
45. Li, J., Li, X., Zhai, H.-J. & Wang, L.-S. Au20: A tetrahedral cluster. *Science* **299**, 864–867 (2003).
46. Chai, J.-D. & Gordon-Head, M. Long-range corrected hybrid density functionals with damped atom-atom dispersion corrections. *Phys. Chem. Chem. Phys.* **10**, 6615–6620 (2008).
47. Weigend, F. & Ahlrichs, R. Balanced basis sets of split valence, triple zeta valence and quadruple zeta valence quality for H to Rn: Design and assessment of accuracy. *Phys. Chem. Chem. Phys.* **7**, 3297 (2005).
48. Frisch, M. J. *et al. Gaussian 16, Revision B. 01* (2016).
49. Boys, S. F. & Bernardi, F. The calculation of small molecular interactions by the differences of separate total energies. Some procedures with reduced errors. *Mol. Phys.* **19**, 553–566 (1970).
50. Marenich, A. V., Cramer, C. J. & Truhlar, D. G. Universal solvation model based on solute electron density and on a continuum model of the solvent defined by the bulk dielectric constant and atomic surface tensions. *J. Phys. Chem. B* **113**, 6378–6396 (2009).
51. Bigeleisen, J. & Wolfsberg, M. Theoretical and experimental aspects of isotope effects in chemical kinetics. In *Advances in Chemical Physics* 15–76 (Wiley, 1957).
52. Anisimov, V. & Paneth, P. ISOEFF98. A program for studies of isotope effects using hessian modifications. *J. Math. Chem.* **26**, 75–86 (1999).
53. Kříž, K., Nováček, M. & Řezáč, J. Non-covalent interactions atlas benchmark data sets 3: Repulsive contacts. *J. Chem. Theory Comput.* **17**, 1548–1561 (2021).
54. Neklyudov, V. & Freger, V. Water and ion transfer to narrow carbon nanotubes: Roles of exterior and interior. *J. Phys. Chem. Lett.* **12**, 185–190 (2021).
55. Aydin, F. *et al.* Ion solvation and transport in narrow carbon nanotubes: Effects of polarizability, cation−π interaction, and confinement. *J. Chem. Theory Comput.* **17**, 1596–1605 (2021).
56. Stanisky, C. M. *et al.* Helium entry and escape through a chemically opened window in a fullerene. *J. Am. Chem. Soc.* **127**, 299–302 (2005).
57. Murata, M., Murata, Y. & Komatsu, K. Surgery of fullerenes. *Chem. Commun.* https://doi.org/10.1039/b811738a (2008).
58. Saunders, M., Jiménez-Vázquez, H. A., Cross, R. J. & Poreda, R. J. Stable compounds of helium and neon: He@C60 and Ne@C60. *Science* **259**, 1428–1430 (1993).

Acknowledgements

Partial support by the grant MAB PLUS/11/2019 from the Foundation for Polish Science and computer time allocation at PL-GRID via Cyfronet, Kraków, Poland are gratefully acknowledged. This work has been completed while the first author was Doctoral Candidate in the Interdisciplinary Doctoral School at the Lodz University of Technology, Poland.

Author contributions

Methodology, P.P, M.P.; investigation, A. P., P.P., and M.P.; writing-original draft preparation, P.P., M.P.; writing-review and editing, A.P., P.P., and M.P; visualization, P.P.; supervision, P.P. All authors have read and agreed to the published version of the manuscript.

Competing interests

The authors declare no competing interests.

Additional information

Supplementary Information The online version contains supplementary material available at https://doi.org/10.1038/s41598-022-05629-6.

Correspondence and requests for materials should be addressed to P.P.

Reprints and permissions information is available at www.nature.com/reprints.

Publisher's note Springer Nature remains neutral with regard to jurisdictional claims in published maps and institutional affiliations.